DOI: 10.2478/jlecol-2026-0038 Journal of Landscape Ecology (2026), Vol: 19 / No. 4

URBAN INFLUENCE ON LANDSCAPE TRANSFORMATION AND LAND COVER INTERACTIONS DURING URBAN EXPANSION (1972–2022): A REMOTE SENSING AND GIS-BASED ANALYSIS

AMINA KALBAZA[1*], BELKACEM MARIR[2] AND FARIDA NACEUR[3]

[1]*Child, City and Environment Laboratory of LEVE of Hadj Lakhdar Batna1 University, Institute of Architecture and Urban Planning, Hadj Lakhdar Batna1 University, Batna 05000, Algeria, amina.kalbaza@univ-batna.dz*
[2]*Urban Planning and Transport Laboratory: Habitat, Landscape and Urban Mobility of Hadj Lakhdar Batna1 University, Institute of Architecture and Urban Planning, Hadj Lakhdar Batna1 University, Batna 05000, Algeria, email: belkacem.marir@univ-batna.dz*
[3]*Urban Planning and Transport Laboratory: Habitat, Landscape and Urban Mobility of Hadj Lakhdar Batna1 University, Institute of Architecture and Urban Planning, Hadj Lakhdar Batna1 University, Batna 05000, Algeria, email: farida.naceur@univ-batna.dz*
**Corresponding author email: amina.kalbaza@univ-batna.dz*

Received: 9th November 2025, **Accepted:** 12th May 2026

ABSTRACT

This study investigates how urban expansion influences land cover dynamics. An interactive analytical approach was adopted to examine the transitions among built-up areas, cropland, and bare land throughout the urbanization process. Remote Sensing and GIS techniques, in conjunction with the Land Transfer Matrix (LTM), Landscape Metrics (LM), Multi-buffer Ring (MBR) and complementary spatial tools, were employed to analyze the city of Tiaret in Algeria over the past half century (1972-2022). The results reveal a marked intensification of urbanization, with an Overall Average Annual Urban Expansion Rate (OA-AUER) of 28.3 ha and a concurrent rise in bare land driven by cropland conversion under urban pressure. Notably, 89.4 % of cropland loss initially transitions into bare land, while subsequent urban development originates from cropland (52 %) and bare land (47 %). The observed density patterns in peripheral areas confirm the significant influence of the urban core on surrounding land-cover transformations. These findings elucidate the urbanization process while considering the transitional role of bare land and further explain diffusion coalescence process. Further empirical research is recommended to refine theoretical frameworks on landscape transformation dynamics and to inform policies aimed at mitigating bare-land expansion in peri-urban areas, controlling cropland urbanization, and planning sustainable urban growth.

Keywords: urbanization; cropland; bare land, remote sensing, GIS technologies.

INTRODUCTION

The efficient planning of urban growth that safeguards ecosystem services has become a global imperative (Abu Hatab *et al*., 2019; Yuan *et al*., 2019), particularly as urbanization emerges as one of the defining demographic megatrends of the twenty-first century (United Nation, 2019). Research on Land Cover Change (LCC) indicates that urbanization has been a major driver of global land surface transformations (Turner *et al*., 2007; Sharma *et al*., 2024), accounting for approximately 60 % of these changes (Song *et al*., 2018). As a complex socio-economic process that restructures rural settlements into urban entities, urbanization induces profound alterations in agroecosystems (Deng *et al*., 2011; Yameogo, 2021). A particularly concerning outcome is cropland degradation, primarily through fragmentation (Gomes *et al*., 2019; Yuan *et al*., 2022) and loss (Qiu *et al*., 2020; Xie *et al*., 2023), which directly threatens global food security (Raphael & Ukandu, 2015; Hossain *et al*., 2020). Cropland fragmentation diminishes agricultural productivity (Deng *et al*., 2011), with peri-urban farmland increasingly subdivided into smaller and less viable parcels (Akın & Erdoğan, 2020; Eko & Ayama, 2013). D'Amour *et al*. (2017) project that highly productive agricultural land, approximately 1.77 times more fertile than the global average, is likely to be lost by 2030, predominantly in Asia and Africa, due to continued urban expansion.

The conversion of cropland to urban uses occurs through the diffusion-coalescence process of urbanization. This process represents a cyclical pattern of urban growth in which new built-up patches initially expand in a dispersed manner during the diffusion phase and subsequently merge into continuous urban forms during the coalescence phase (Tian & Wu, 2015). This dynamic, often resulting from weak land-use planning (Li *et al*., 2017b), exacerbates landscape fragmentation in peri-urban areas, particularly during the diffusion stage, and leads to spatial dispersal and unesthetic urban forms (Banai & DePriest, 2014; Ewing, 1997). The negative consequences of such urbanization include intensified land speculation and aggravated land-use conflicts (Peerzado *et al*., 2019), which further complicate sustainable urban management and spatial planning efforts aimed at reconciling urban development with environmental sustainability.

The integration of Remote Sensing (RS) and Geographic Information Systems (GIS) has enabled the systematic monitoring and quantification of urban expansion (Turner *et al*., 2007). Although the interrelations among urban growth, bare land expansion, and cropland decline are acknowledged (Abu Hatab *et al*., 2019; Li *et al*., 2017a), they are frequently examined independently. Most existing studies emphasize the rate of cropland loss resulting from urbanization (Gumma *et al*., 2017; Wang *et al*., 2015; Zhou *et al*., 2014), conceptualizing it as a direct and unidirectional process. Only a limited number have examined the interconnected and bidirectional dynamics linking urban expansion and cropland conversion (Tu *et al*., 2021, 2023), the relationship between urbanization and bare land growth (Dadashpoor *et al*., 2019; Zhou *et al*., 2014), or the transitional processes from cropland to bare land under urbanization pressure (Ruiz-Lendínez, 2020). This research investigates how urban expansion shapes landscape transformation by analyzing the interactions among urban areas, cropland, and bare land during the urban expansion process. This study therefore hypothesizes that urban expansion drives cropland loss and increases bare land as a transitional phase.

Our study adopts an interactive analytical approach to investigate the interactions among built-up areas, cropland, and bare land. It further examines the implications of their mutual coexistence for urban growth dynamics, particularly within peri-urban zones where these land cover types intersect, while considering the influence of urban core on these dynamics. Which consists of a municipal-scale study aimed at providing information on the state of urban growth and the characteristics of peripheral areas. The case study focuses on Tiaret, Algeria, a city that has undergone substantial land-cover transformation, particularly the conversion of fertile cropland into urban land, thereby enriching the global urban literature on medium-sized cities within the Maghrebi context, as recommended by previous studies (Chettry, 2023). To ensure temporal robustness, urbanization dynamics are analyzed over the past five decades. The methodological framework integrates Remote Sensing (RS) and Geographic Information System (GIS) technologies with a suite of spatial analytical tools, including the Land Transfer Matrix (LTM), Multi-Buffer Ring (MBR), Standard Deviational Ellipse (SDE), Contribution–Dependence Indices (CDI), and Landscape Metrics (LM). This integrative framework enables a comprehensive understanding of the rate, direction, and spatial configuration of land cover change (LCC) during urbanization process and the impact of the urban core on these changes.

METHODOLOGY

Case of study

The city of Tiaret, located within the administrative boundaries of Tiaret Wilaya in northwestern Algeria, is situated approximately 150 kilometres south of the Mediterranean coastline. Between 1972 and 2020, the population of Tiaret experienced a substantial increase, rising from 64 764 to 262 590 inhabitants. By 2020, urban residents accounted for approximately 99 % of the population, while only 1 % remained in rural areas. This demographic growth is closely linked to the city's urbanization, driven by several key factors: the development of industrial infrastructure during the 1970s, the proliferation of informal settlements in the aftermath of the security crisis of the 1990s, and a series of state-led housing policy interventions. These dynamics have fostered leapfrog urban development, resulting in the spatial integration of conurbations such as Karman and Es-Senia, as well as the establishment of industrial zones as shown in Fig. 1.c. Historically, Tiaret originated as an agricultural village during the colonial period and was officially designated a town in 1856. The city’s agropastoral identity is shaped by its favourable climatic and geomorphological conditions, as well as the complementarity between the highly productive Sersou plains, recognized as one of the most fertile agricultural zones in North Africa and the adjacent steppe regions, depicted in Fig. 1.b. As a result, the wilaya of Tiaret holds a leading position in Algeria in terms of cereal production and ranks third nationally in red meat output (Tiaret Wilaya, 2022).

Fig. 1: Geographic context of the study area: (a, a') Location of Tiaret Wilaya within Algeria; (b) Delimitation of the study area in relation to major geomorphological zones; (c) Spatial distribution of urban centres and conurbations within the study area.

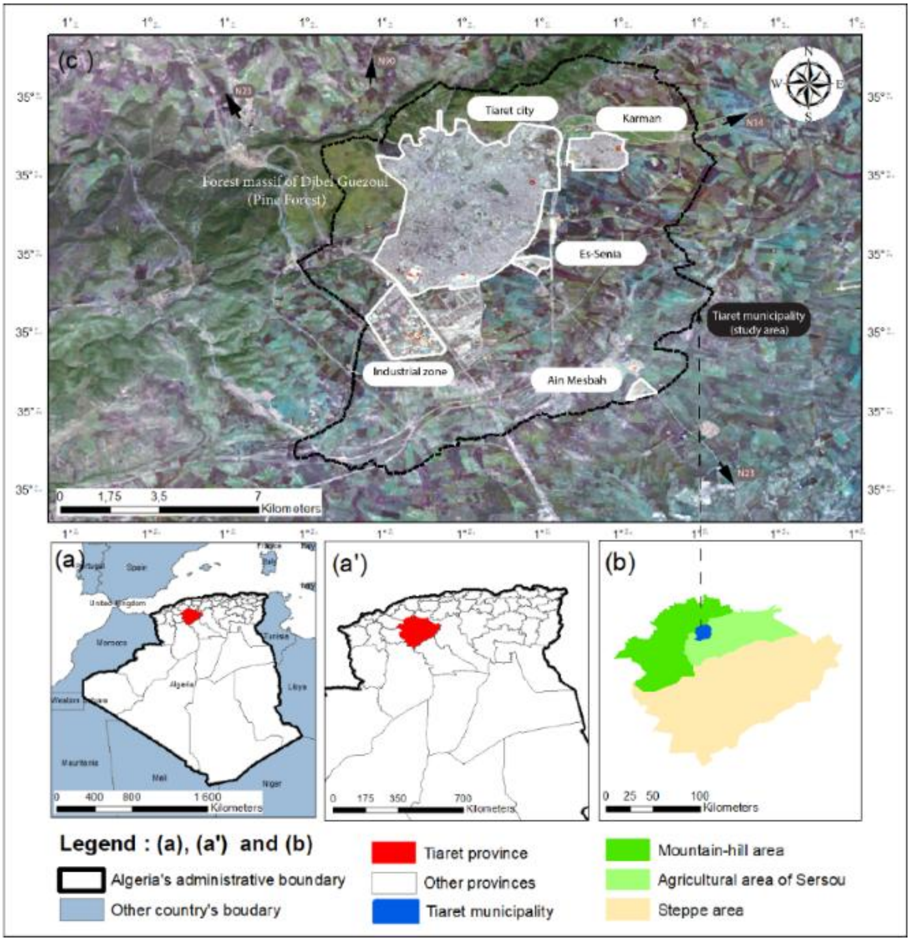

Overall Methodological Workflow

This study investigates the interactions among built-up areas, cropland, and bare land throughout the urbanization process. The methodological framework includes five main components as illustrated in Fig. 2. The study period was divided into five intervals: T1 (1972_1982), T2 (1982_1991), T3 (1991_2002), T4 (2002_2011), and T5 (2011_2022). First, comprehensive data acquisition, preprocessing, and preparation were undertaken to facilitate land cover classification and the generation of Land Cover Maps (LCM). Second, temporal dynamics were quantified through the calculation of land cover change rates, supplemented by Contribution–Dependence Indices (C-DI) to evaluate the mutual dependencies and transitions among land cover categories. Third, spatial displacement patterns of each land class were analyzed using the Standard Deviational Ellipse (SDE) method, including overlap analysis to elucidate interactive movement tendencies. Fourth, landscape metrics (LMs) were computed to assess the extent and nature of landscape fragmentation associated with urbanization. Lastly, a Multi-Buffer Ring (MBR) analysis was employed to evaluate the spatial influence of urban core on surrounding land cover transformations.

Fig. 2: Methodological framework diagram

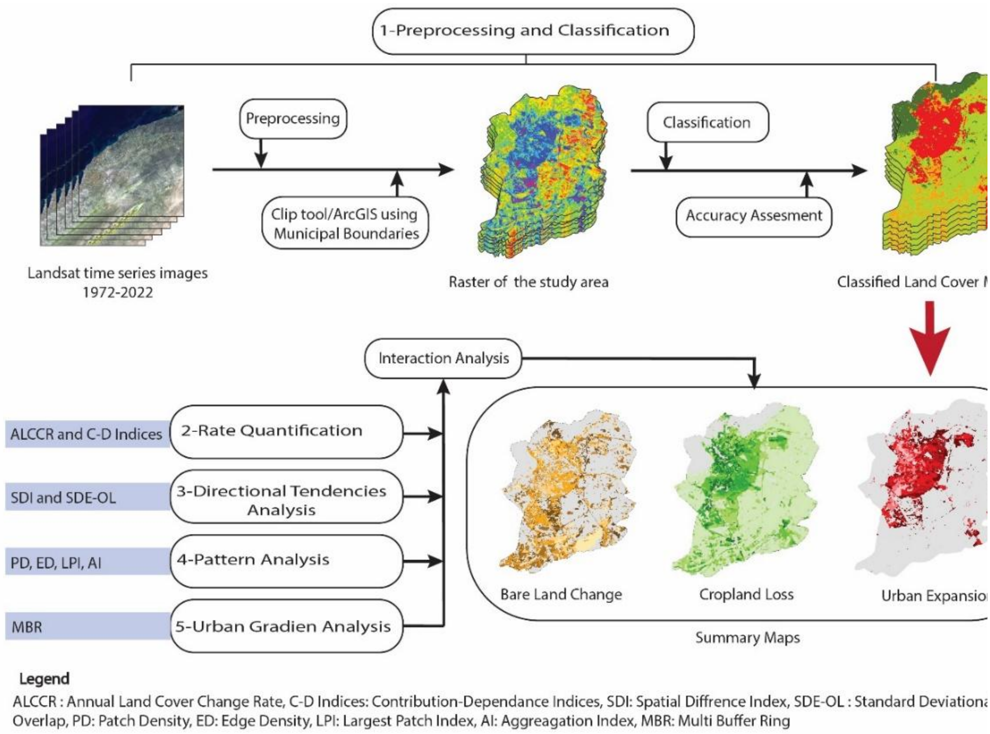

Satellite imagery acquisition and pre-processing

Six Landsat images from 1972 to 2022, one per decade, were selected from the USGS archive based on full coverage, minimal cloud presence, and alignment with the agricultural calendar for most of them. Acquired from MSS, TM, ETM+, and OLI-TIRS sensors, as shown in table 1, the data were processed in ArcGIS using administrative boundaries from Tiaret's 2019 Master Plan. The 1972 (Landsat 1) and 1982 (Landsat 4) were geometrically and radiometrically corrected following the method of Gumma *et al*. (2017). Orthorectification was performed using a Digital Elevation Model (DEM) for terrain correction and Ground Control Points (GCPs) for horizontal alignment, with accuracy assessed from independent GCPs. Radiometric calibration to Top of Atmosphere (TOA) reflectance with solar angle correction was applied using Equation (1), and both images were resampled to 30 m to ensure resolution consistency with the other datasets. Where for Equation (1): $P\lambda$ denotes TOA reflectance, where: Mp and Ap are the band-specific multiplicative and additive rescaling factors respectively, $Qcal$ is the calibrated digital number, and $\emptyset se$ is the local solar elevation angle from the metadata.

$$P\lambda = \frac{Mp \times Qcal + Ap}{sin(\emptyset se)} \quad (1)$$

Table 1: Landsat Imagery used in the Study.

Satellite Platform	Sensor-ID	Spatial Resolution	Acquisition Date
Landsat 1	The Multispectral Scanner (MSS)	60 m	15/11/1972
Landsat 4	The Multispectral Scanner (MSS)	60 m	26/09/1982
Landsat 5	Thematic Mapper (TM)	30 m	03/03/1991
Landsat 7	Enhanced Thematic Mapper (ETM)	30 m	25/03/2002
Landsat 7	Enhanced Thematic Mapper (ETM)	30 m	26/03/2011
Landsat 8	Operational Land Imager and Thermal Infrared Sensor, (OLI-TIRS)	30 m	25/04/2022

Classification

Land cover maps were generated through the supervised classification (Dadashpoor *et al*., 2019) of Landsat imagery via ArcGIS. To improve class separability, following the method of Mosammam *et al*. (2017), we used false colour composites images to support class distinction and guide training sample selection. The quality and quantity of training samples were enhanced by selecting diverse, well-distributed reference points, informed by contextual knowledge of the study area. Remaining confusion was minimized through visual interpretation. Post-classification refinements, including filtering, smoothing, and generalization, were also applied following the methodology of Mosammam *et al*. (2017). Classification accuracy was assessed using an error matrix derived from 200 randomly distributed validation points per image (Abudu *et al*., 2019; Dutta & Das, 2019). Four principal land cover categories were generated: built-up areas, cropland, bare land, and forest. Among these, built-up areas, cropland, and bare land were then extracted for independent analysis. Temporal aggregation of each class facilitated the production of summary maps depicting patterns of urban expansion, cropland loss, and bare land change.

Land cover dynamics analysis

Following the classification, the change rates were computed using Equation (2) (Boori *et al*., 2015; Tang *et al*., 2021). The original equation, commonly applied to quantify urban expansion, was adapted in our study to evaluate the intensity of urban expansion by normalizing the change relative to the total land area at the beginning of the study period. Moreover, absolute values were applied in the equation to calculate change intensity, while negative values were reported to indicate decreases in cases where a land cover class exhibited both gains and losses.

Change detection analysis was conducted using ArcGIS, wherein a Land Transfer Matrix (LTM) was employed to systematically quantify land cover transitions throughout the study period (Yuan *et al*., 2022). To further elucidate the interactions among built-up areas, bare land, and cropland, the Contribution Index (CI) and Dependence Index (DI), as formulated by Tu *et al*. (2021), were employed using Equations (3) and (4). While these indices were originally designed to assess the interactions between built-up areas and cropland, they were modified in this study such that the denominator accounts for all land cover types involved in the transfer, reflecting the inclusion of three land cover classes in the analysis. The dependence index (DI) quantifies the percentage to which the growth of class a depends on class b, whereas the contribution index (CI) measures the percentage contribution of class b to the loss or gain of class a. These indices provided a comprehensive assessment of the reciprocal influences among land cover categories, thereby offering insights into the underlying dynamics of urbanization.

$$ALCCR = \frac{|LA_{n+i} - LA_i|}{n \times TLA_{ref}} * 100 \tag{2}$$

$$CI = \frac{T_{x \to y}}{\sum T_{x \to z}} * 100 \tag{3}$$

$$DI = \frac{T_{x \to y}}{\sum T_{z \to y}} * 100 \tag{4}$$

Where: For Equation (2): $ALCCR$ is the Annual Land Cover Change Rate, where: LA_i and LA_{n+i} are the land area of a given class at time i and $n + i$ respectively, n is the time interval in years and TLA_{ref} is the reference total land area at the beginning of the study. For Equations (3) and (4): $T_{x \to y}$ is the total area converted from type x to y, $\sum T_{x \to z}$ is the area of x converted to all other types z (where $z \# x$) and $\sum T_{z \to y}$ is the area transferred to y from all other types z (where $z \# x$).

Standard deviational ellipse

The Standard Deviation Ellipse (SDE) is employed to identify the directional trend of spatial distributions, wherein the ellipse's centroid represents the spatial gravity center of the features, and its major and minor axes denote the orientation and concentration of spatial patterns, respectively. To assess temporal shifts in the directional tendencies of built-up areas, cropland, and bare land, we applied both the Spatial Difference Index (SDI) and the SDE-based Overlap Index (SDE-OL). The SDI, calculated using Equation (5), measures the degree of spatial divergence between distributions, with values ranging from 0 to 1; higher values indicating greater spatial disparity (Tang et al., 2021).

The SDE-OL, calculated using Equation (6), is developed in this research to captures spatial interaction by quantifying the degree of overlap between ellipses representing different land cover types over time, where higher index values reflect stronger spatial association. Together, SDI and SDE-OL provide a comprehensive framework for analyzing land cover dynamics by integrating directional tendencies with spatial interaction patterns.

$$SDI = -\frac{\text{Area (SDEa} \cap \text{SDEb)}}{\text{Area (SDEa} \cup \text{SDEb)}} \tag{5}$$

$$SDE.OL = \frac{Ao}{\text{A}^1 + \text{A}^2 - \text{Ao}} * 100 \tag{6}$$

Where: For Equation (5): $\text{Area (SDEa} \cap \text{SDEb)}$ is the area of intersection of the two ellipses (a) and (b), respectively and $\text{Area (SDEa} \cup \text{SDEb)}$ is the area of their union. For Equation (6): Ao is the overlap area of the two ellipses, A^1 and A^2 are the area of the ellipses corresponding to the two land cover categories.

Landscape metrics

Landscape metrics were computed to assess the spatial fragmentation of built-up areas, cropland, and bare land, following the methodologies of Magidi &Ahmed (2019), Akın & Erdoğan (2020) and Tu *et al*. (2021). The analysis was conducted using FRAGSTATS software. Key metrics included Patch Density (PD), Edge Density (ED), Largest Patch Index

(LPI), and Aggregation Index (AI), reflecting fragmentation, edge complexity, dominance, and aggregation, respectively, as explained in Table 2.

Table 2: Explanation of Landscape Metrics.

Landscape metrics	Description	Range	Unit	Measure
Patch density PD	The number of patches per unit area. Higher values indicate greater fragmentation.	PD > 0, constrained by cell size	Number per 100 hectares	Fragmentation
Edge density ED	The total length of all edge segments per unit area. Higher values indicate more irregularity and fragmentation.	ED≥0, without limit	Meter per hectare	Complexity of the fragmentation
Largest patch index LPI	The perimeter-to-area ratio of the largest patch relative to the entire landscape. Higher values indicate dominance of a single large patch, while a low LPI indicates fragmentation.	0 < LPI ≤100	Percent	Dominance
Aggregation index	The number of like-adjacencies relative to the maximum possible like-adjacencies. Higher values indicate stronger spatial continuity, while lower a low of AI indicates fragmentation.	0 < AI ≤100	Percent	Aggregation

Multi-Buffer Ring (MBR) analysis

Usually, the multi-buffer ring (MBR) method is employed to analyze the urban-rural gradient density. In this study, it was applied to evaluate land cover changes and the interactions among built-up areas, cropland, and bare land across spatial gradients, considering the influence of the urban core. The urban core of La Redoute (35°22'38.65"N, 1°19'2.53"E) was selected as the central reference point. Around this core, seven concentric buffer zones were generated at 1 km intervals, encompassing both the original urban agglomeration and its peripheral expansion zones to capture the spatial dynamics of urban expansion. The density of each land cover class, built-up areas, cropland, and bare land, was calculated within each buffer ring using Equation (7).

$$RD = \frac{LCA}{\mathrm{TA}} \qquad (7)$$

Where: RD is the ring density, where: LCA is the land cover area within the buffer, and TA is the total ring area.

RESULTS AND DISCUSSIONS

Accuracy assessment results

Orthorectification accuracy yielded Root Mean Square Error (RMSE) values of 7.4 m for the 1972 image and 4.9 m for the 1982 image, both within acceptable limits, with residual errors below 0.5 pixels (Deng *et al*., 2011).Visual checks of well-defined features such as roads further confirmed the minimal spatial misalignment through the absence of noticeable distortions between the orthorectified images and the reference data. Classification accuracy, evaluated using an error matrix (Abudu *et al*., 2019) showed overall accuracy (OA), Kappa Index of Agreement (KIA), Producer's Accuracy (PA), and User's Accuracy (UA), all presented in Table 3, consistently exceeding 0.90, with KIA ranging from 0.94 to 0.98, indicating excellent agreement and confirming the high reliability of the classification (Mosammam *et al*., 2017).

Table 3: Classification accuracy assessment results.

Year	User's accuracy			Producer's accuracy			Overall Accuracy (OA)	Kappa Index of Agreement (KIA)
	Cropland	Built-up areas	Bare land	Cropland	Built-up areas	Bare land		
1972	0.98	1	1	1	1	0.75	0.98	0.94
1982	0.99	0.80	1	1	1	0.74	0.98	0.94
1991	0.99	0.90	1	1	1	0.92	0.98	0.95
2002	0.98	1	1	1	1	0.91	0.98	0.96
2011	0.98	1	0.93	0.98	0.96	1	0.98	0.96
2022	0.99	1	1	0.99	1	0.97	0.99	0.98

The effect of urban expansion on global land cover changes

Fig. 3 shows the temporal trends in land cover change across six periods from 1972 to 2022. Fig. 4 illustrates land cover dynamics over the study period through classification maps and summary maps depicting urban expansion, cropland loss, and bare land change, each tracing the evolution of the corresponding SDE. While Table 4 complements these visualizations by presenting the calculated rates, SDI and SDE.OL results for the three analysed land cover classes. The results indicate an expansion of the built-up area, totalling 2339 ha, while cropland declined by 3878 ha and bare land increased by 1480 ha. The respective overall average annual change rates were 28.3 ha/year for built-up areas, 1.2 ha/year for cropland loss, and 8.2 ha/year bare land increase, with a slight decline in bare land observed during T5. The Annual Urban Expansion Rate (AUER) rose from 17.5 in T1 to 47.6 in T5, while the Annual Cropland Loss Rate (ACLR) peaked at 1.6 in T2 before falling to 0.9 in T5. The Annual Bare Land Increase Rate (ABLIR) showed temporal variability.

Fig. 3: Temporal trends in land cover change across six periods from 1972 to 2022

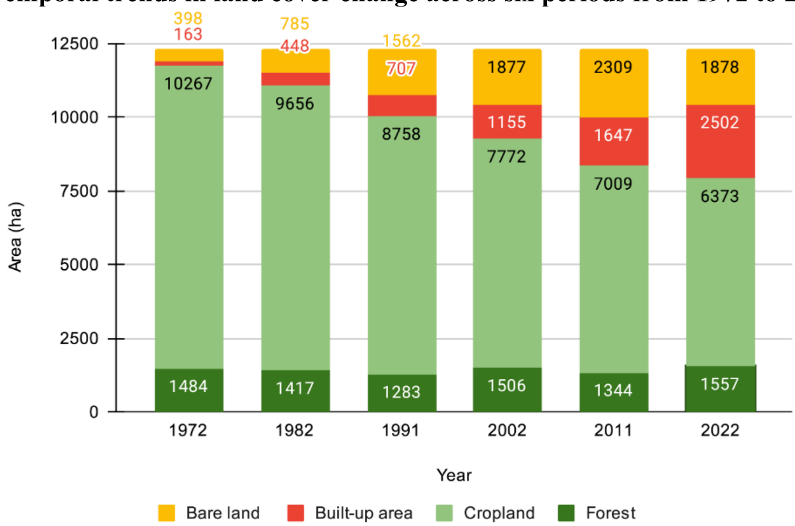

Considering urbanization, the annual change remains minimal compared to other large cities, such as Kuala Lumpur, which recorded an annual increase of 243.5 ha/year from 1989 to 2014 (Boori *et al*., 2015), or Barcelona, which recorded 887 ha/year during 1956-1997 (Paül & Tonts, 2005). This reflects the medium sized character of Tiaret. It should be noted that our calculated annual change covers a relatively long period of 50 years, during which the intensity of urbanization may have varied across different phases. Nevertheless, the extent of urbanization remains limited compared to major cities worldwide. Therefore, investigating the spatial implications of this growth is important for advancing the literature on medium sized cities and further raises concerns about the contribution of medium sized cities to global urbanization and landscape transformation.

With regard to cropland loss, the overall average annual cropland loss rate (OA-ACLR) in Tiaret, estimated at 1.2 ha/year and reported in Table 4, remains considerably lower than the average value reported for the 14 Chinese cities, approximately 100 ha/year (Tu *et al*., 2021). Considering that Chinese cities are among the most highly urbanized in the world, the cropland loss rate in Tiaret represents only 1.2 % of the average observed in these cities. However, despite this lower rate, medium sized cities remain important to investigate, as their large number contributes significantly to global cropland decline, and their cumulative cropland conversion can become substantial when aggregated. In this regard, medium sized cities can collectively rival megacities in total contribution to cropland loss at the global scale. This comparison is based solely on a rate indicator, which, as a mathematical measure, does not fully capture the complexity of cropland loss processes, including land availability, and agricultural structure. While the Tiaret region is widely recognized for its significant cereal production potential, the persistent loss of cropland represents a critical challenge, particularly for food security, given that cereals constitute a major staple in North Africa, where arable land is unevenly distributed and not widely available across all countries. Therefore, public authorities should reconsider urban development strategies that have contributed to substantial agricultural land loss and adopt more proactive planning approaches that integrate surrounding cropland while preserving rural areas, in order to strengthen food security (Hossain *et al*., 2020).

The general land cover dynamics in the study area reveal that urban expansion initially coincided with substantial cropland loss referring to the diffusion process, with the Annual Cropland Loss Rate (ACLR) peaking in T2, followed by a more gradual decline indicative of urban coalescence. This pattern underscores a strong correlation between urban growth and cropland conversion. These patterns additionally align with Fig. 4, which shows substantial urban expansion during T1 and T2, driven by a diffusion process, covering the adjacent cropland to urban areas in the southwest and bare land in the southeast. In contrast, T3, T4, and T5 illustrate a coalescence process, characterized by the merging of urban patches to form a more consolidated spatial pattern.

With regard to bare land change, cropland loss stems from indirect effects of urbanization (Ruiz-Lendínez, 2020), including land speculation, abandonment, and policy-driven reallocation, as well as from natural factors such as soil degradation and fertility decline. Consequently, the overall rise in bare land is linked to cropland abandonment, driven by the combined influences of urban encroachment and land degradation. The calculated rates, as presented in Table 4, indicate temporal fluctuations in ABLIR likely reflect construction cycles, with peaks corresponding to land clearing and cropland fallowing. These findings correspond to the observation that cropland is consistently under pressure in the urban fringe, undergoing a process of abandonment in anticipation of future urban development (Ruiz-Lendínez, 2020). During a construction cycle, bare land increases as a result of cropland abandonment and its transformation into bare land, and then decreases when this bare land is converted into urban areas, with this decline marking the beginning of a new construction cycle. This phenomenon is evidenced by the ABLIR, which reflects two construction cycles with increases in T2 and T4, as shown in Table 4.

Fig. 4: Land use classification maps and Summary Maps with Standard Deviational Ellipse of Tiaret municipality across six time periods between 1972 and 2022.

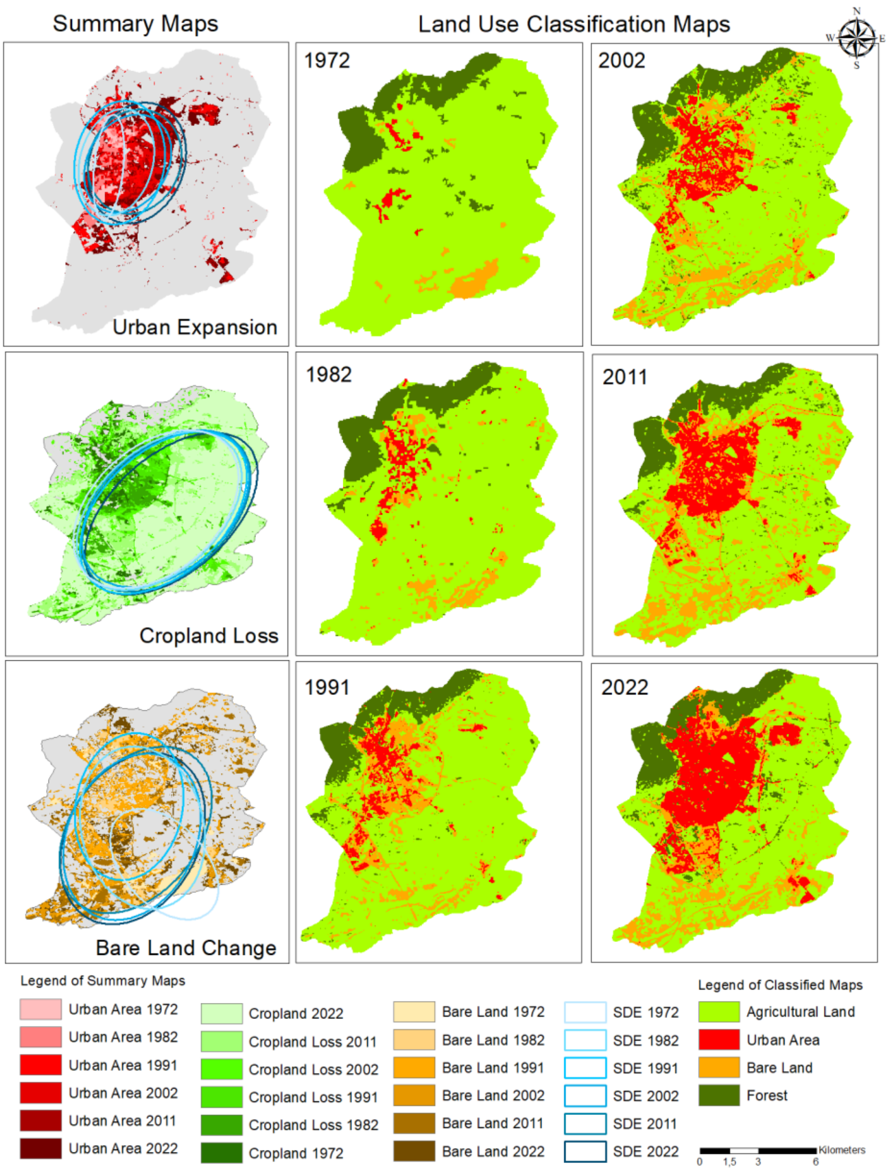

The overall land cover dynamics, including built-up areas, cropland, and bare land, provide valuable insights into the pursuit of urbanization and offer information on the diffusion-coalescence process, thereby contributing to a better understanding of the city's urban growth stage. The knowledge derived from analyzing interactions among urban areas, cropland, and bare land is essential for informed decision-making for guiding urban development, particularly amid rising global urbanization, taking into account both environmental impacts and the city's spatial characteristics. For instance, the diffusion phase often reflects a fragmented urban pattern in peripheral areas and an extensive conversion of cropland, necessitating strong planning interventions.

Table 4: Quantitative assessment of land cover change rates, Spatial Difference Indices (SDI) and Standard Deviational Ellipse Overlap indices

Period	Rate calculation						Directional tendencies					
	Urban expansion		Cropland loss		Bare land increase		SDI			SDE.OL		
	AUE (ha/y)	AUER (%)	ACL (ha/y)	ACLR (%)	ABLI (ha/y)	ABLIR (%)	Urban Areas	Bare land	Cropland	Urban/ cropland	Urba n/bar e land	Cropland /bare land
T1 (1972-1982)	28.5	17,5	61.1	1	38.7	9.7	0.7	0.7	0.5	14.6	64.1	61.5
T2 (1982-1991)	28.8	17,7	99.8	1.6	86.3	21.7	0.6	0.6	0.5	17.3	43	44.5
T3 (1991-2002)	40.7	25	89.6	1.4	28.6	7.2	0.6	0.6	0.5	18.9	24	54.6
T4 (2002-2011)	54.7	33,5	84.8	1.3	48	12.1	0.6	0.5	0.5	21.2	26.4	62.6
T5 (2011-2022)	77.7	47,7	57.8	0.9	-39.2	-9.8	0.6	0.5	0.5	20.6	29.1	52.4
Overall Average (OA)	**46.1**	**28.3**	**78.3**	**1.2**	**32.5**	**8.2**	**0.6**	**0.5**	**0.6**	**18.5**	**37.3**	**55.1**

Interactions among Land Cover Types through Their Contribution and Dependence during Urban Expansion

Results of contribution-dependence indices (CDI) indicate the following: The Cropland-to-Urban Dependence Index (CU. DI) and Bare Land-to-Urban Dependence Index (BU. DI) were 52 % and 47 %, respectively; the Cropland-to-Bare Land Dependence Index (CB. DI) reached 89.4 %. The CU. DI aligns with Yuan *et al*. (2022), who reported 49.26 %, which is consistent with the observation that nearly half of the urban areas originate directly from cropland. For cropland loss pathways, the Cropland-to-Urban Contribution Index (CU.CI) was 25.2 % and the Cropland-to-Bare land Contribution Index (CB.CI) was 74.8 %. The CU.CI is consistent with the average value of 27.78% observed across the nine agricultural zones in China (Tu *et al*., 2023). The Bare Land-to-Urban Contribution Index (BU.CI) reached 37.9 %, consistent with Ruiz-Lendínez (2020), who noted 40.3 % abandonment within urban boundaries.

CDI results demonstrate that bare land expansion largely stems from cropland degradation, while urban growth draws almost equally from cropland and bare land. These results are consistent with previous findings in the Tabriz Metropolitan Area, where most ecological lands were transformed into bare land and urban areas (Dadashpoor *et al*., 2019). Notably, cropland often follows a two-stage trajectory, first degrading into bare land, then undergoing urbanization through coalescence. In contrast, direct cropland-to-built-up area conversion is more typical of diffusion-driven expansion. Only about 25 % of cropland is directly urbanized, with most transitioning into built-up areas following degradation. These findings reveal a complex, multi-phased land transformation process, wherein cropland functions both as a direct source and an intermediate stage in urban expansion, shaped by degradation and land cover change. It is worth noting that our results are consistent with previous studies, even though CDI does not appear to have been explicitly applied in most studies, except in a study conducted in China (Tu *et al*., 2023) where CDI was developed and applied without incorporating bare land change. These findings highlight the need for further global-scale investigations to validate and reinforce these results, as well as to extend analyses to studies examining the interactions among urban areas, cropland, and bare land. Especially since this knowledge provides valuable insights into land cover dynamics, including the cropland urbanization process, and calls for greater attention to bare land management on city outskirts.

Directional Trends in Land Cover Dynamics during Urban Expansion

SDE results, presented in Table 4, reveal that the values of SDI for built-up areas remained above 0.5, cropland stabilized around 0.5, and bare land initially exceeded 0.5 but declined to 0.5 by T4-T5. Whereas SDE.OL values show increasing built-up areas-cropland spatial interaction, cropland-bare land interactions fluctuated. Built-up areas-bare land SDE.OL declined from T1 to T3 before rising again in T4 and T5. The overall values of SDE.OL for the three land cover types ranged from 0 % to 67 % on a three-range percentage scale.

Regarding directional tendencies, results of SDI reveal substantial spatial reconfiguration driven by urban expansion, including the relocation of nearly half the cropland, a transition marked by spatial displacement while partially maintaining historical continuity. These results are consistent with our previous findings on land cover dynamics, with the high OA-ACLR indicating substantial cropland consumption. Bare land exhibited significant spatial dispersion aligned with early urban growth phases, followed by relative stabilization.

SDE.OL results indicates progressive cropland loss due to urban encroachment, and unstable dynamics between cropland and bare land likely shaped by both environmental variability and anthropogenic factors. Minimal interaction between built-up areas and bare land was observed in T1 to T3, whereas higher interaction in T4 and T5 reflects intensified urban encroachment into previously undeveloped or transitional zones, likely linked to infrastructure and housing development.

Overall, a moderate level of spatial overlap among the three land cover types suggests gradual rather than abrupt land conversion processes. The average SDE.OL between cropland and bare land exceeded those involving built-up areas, indicating a stronger spatial interaction and underscoring the mediating role of bare land in cropland urbanization. Initially, bare land expanded primarily through cropland degradation; in later stages, increased overlap with built-up areas suggests the urbanization of bare lands.

The results of directional tendencies further corroborate the global land cover dynamics observed during urban expansion, highlighting that the city's growth process involves both cropland and bare land. Moreover, the interaction between built-up areas and bare land provides insight into the degree of urban densification, indicating the extent to which the city expands by converting adjacent bare land rather than encroaching on cropland. Consequently, the strong interaction between urban areas and cropland, compared with bare land, as observed in Tiaret during T1 to T3, calls for urgent planning intervention, as it reflects increasing pressure on agroecosystems, accelerates productive cropland loss, threatens food security, and raises major concerns regarding environmental sustainability and sustainable land management.

Spatial patterns of land cover during urban expansion

Fig. 5 presents the temporal evolution from 1972 to 2022 of four key landscape metrics: Patch Density (PD), Edge Density (ED), Largest Patch Index (LPI), and Aggregation Index (AI). Overall, PD increased for all land cover classes, reaching 2.4 for built-up areas, 3.7 for cropland, and 6.6 for bare land, patches/100 ha by T5, despite temporary declines in T3 and T4. Built-up areas ED rose steadily to 22.4 m/ha in T5, while cropland and bare land peaked at 58.1 in T3 and 55.2 in T4 m/ha, respectively, before declining. Built-up areas LPI increased to 15.7 % in T5, whereas cropland LPI declined overall, with a slight rise in T5, and bare land LPI fluctuated. AI for built-up areas dropped in T2 but rose to 92.2 % in T5, cropland AI remained stable, and bare land AI showed fluctuations.

Results of LM illustrated indicate the following: First, observed peak in Patch Density (PD) reflects intensified landscape fragmentation, initially driven by cropland fragmentation followed by bare land subdivision. This upward trend in PD indicates a reinforcing fragmentation dynamic under urbanization pressure, while the interim decline likely signals a temporary slowdown in urban growth. The consistently higher PD in bare land compared to cropland supports the idea that cropland is initially subdivided into fragmented bare land parcels. Noting that many previous studies highlight cropland fragmentation under urban pressure (Deng *et al*., 2011; Yuan *et al*., 2022), our results link this fragmentation to the broader process of landscape transformation driven by urbanization.

Second, the increase in Edge Density (ED) denotes growing spatial complexity linked to urban expansion. Peaks in cropland and bare land ED values correspond to periods of heightened fragmentation, followed by phases of stabilization or consolidation. Third, the rise in the Largest Patch Index (LPI) for built-up areas reflects the merging of dispersed patches into a more contiguous urban fabric, whereas the overall decline LPI for cropland indicates continued fragmentation, likely driven by urban encroachment and environmental stressors, with the slight rise in T5 reflecting reduced fragmentation. The fluctuating LPI of bare land reveals its transitional and unstable character, shaped by both fragmentation and repurposing, either via urban integration or ongoing conversion from cropland.

Fig. 5: Variation in Landscape Metrics across the study period.

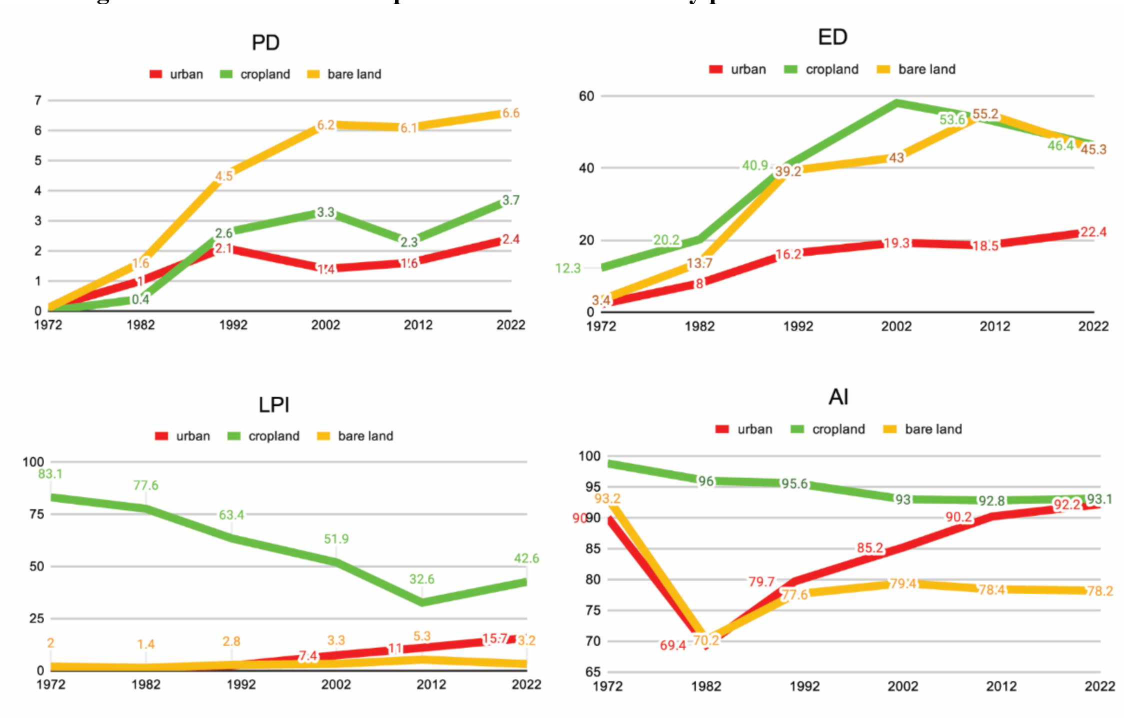

Fourth, the decline in the Aggregation Index (AI) for built-up areas during T2 suggests early-stage fragmentation, while the subsequent increase by T5 indicates coalescence into more aggregated urban forms. In contrast, the stable AI for cropland implies that the remaining agricultural areas maintained a clustered configuration despite partial urban loss. The fluctuating AI of bare land aligns with its intermediary role in urbanization: declining during fragmentation phases and increasing when larger patches emerged from cropland degradation. These patterns are consistent with findings by Dadashpoor *et al*. (2019), who reported intensified landscape fragmentation under urbanization. Their study revealed that areas adjacent to urban expansion exhibited a more fragmented landscape pattern than outer zones, where landscape structures tended to become more clustered. This finding aligns with our results, which indicate pronounced fragmentation on the city outskirts involving both cropland and bare land, likely driven by ongoing urbanization processes. Collectively, the interplay among LM in this study underscores urbanization as a key driver of spatial restructuring and fragmentation of pre-existing land cover types. This shows that the spatial effects of urbanization extend beyond urban areas, as evidenced by previous studies reporting fragmented patterns linked to urban sprawl, affecting rural areas adjacent to urban zones.

Results of multi buffer ring

Table 5 presents the results of the MBR analysis, illustrating the temporal dynamics in the density of built-up areas, cropland, and bare land from 1972 to 2022 within the urban area of Tiaret. These results indicate that built-up area density increased throughout the period, with inner rings consistently denser than outer ones, rising in the first ring from 5.89 m^2/ha in T1 to 26.90 m^2/ha in T5. Cropland density declined overall, with sharper losses in inner rings, dropping from 7468.20 m^2/ha, 6179.75 m^2/ha and 4309.28 m^2/ha in T1 to 215.74 m^2/ha, 593.70 m^2/ha and 551.15 m^2/ha by T5 in the first, second and third rings, respectively. Bare land density showed dynamic patterns, with inner rings peaking earlier in T2 at 2763.92 m^2/ha, 2733.79 m^2/ha, 1514.20 m^2/ha, and 1273.86 m^2/ha before declining, whereas the fifth to seventh rings peaked later in T4 at 786.42 m^2/ha, 614.87 m^2/ha, and 692.43 m^2/ha, respectively, then decreased.

Urban density trends reveal a persistent concentration of development within the core, as evidenced by the continuous increase in the first ring's density. The rise in the second and third rings reflects ongoing suburban densification. Notably, the absence of urban density in the third and seventh rings in 1972 indicates their initial non-urbanized condition. The third ring acted as a transition zone between the initial urban development originating from the city core and the outer urban expansion, which was subsequently driven primarily by the establishment of industrial zones in Tiaret. These patterns suggest a dual process of core densification and peripheral low-density expansion, indicative of urban sprawl (Mosammam *et al*., 2017), alongside a centripetal trend toward compactness within the urban core. Cropland density patterns illustrate a progressive conversion to built-up areas, with the most pronounced losses occurring in central zones and gradually decreasing toward the periphery. Bare land density trajectories reflect a transitional pathway, emerging from degraded cropland and later converted to built-up areas. This progression began in inner rings and advanced outward, consistent with prior findings (Abudu *et al*., 2019; Li *et al*., 2017a) identifying bare land as a precursor to urban growth. And the findings identify urbanization as a key driving force of fragmentation in rural areas adjacent to urban zones (Dadashpoor *et al*., 2019), with our results providing detailed information on fragmentation patterns across different land cover types in the rural urban interface and on the process of cropland transformation into urban areas. Our results confirm the influence of the urban core on land cover dynamics in peripheral areas, highlighting the sequential conversion of cropland to bare land and subsequently to urban areas during peripheral expansion.

Table 5: Temporal dynamics in the density of built-up areas, cropland, and bare land from 1972 to 2022 within the urban area of Tiaret.

Ring number	Class	1972	1982	1991	2002	2011	2022	Increase in the density of urban areas	Decrease in the density of agricultural land
1	**Built-up areas**	5,89	11,36	14,99	16,74	20,88	26,90	**21,01**	
	Cropland	7468,20	4146,08	1209,05	2913,46	945,84	215,74		**7252,46**
	Bare land	498,16	2008,54	**2763,92**	1632,15	2266,15	834,46		
2	**Built-up areas**	0,21	1,31	1,76	2,60	3,35	4,94	**4,73**	
	Cropland	6179,75	4188,47	2596,38	2733,97	1971,84	593,70		**5586,05**
	Bare land	81,61	959,83	**2733,79**	1558,00	1778,54	1164,33		
3	**Built-up areas**	0,0	0,27	0,39	1,08	1,79	2,30	**2,30**	
	Cropland	4309,28	3853,79	2740,89	2165,65	1240,78	551,15		**3758,13**
	Bare land	90,79	240,23	**1514,20**	835,47	821,38	547,95		
4	**Built-up areas**	0,11	0,10	0,20	0,57	0,86	1,21	**1,10**	
	Cropland	4374,00	3960,08	3017,88	2555,88	2034,70	1246,17		**3127,83**
	Bare land	31,63	416,30	**1273,86**	803,22	862,12	606,14		
5	**Built-up areas**	0,02	0,05	0,06	0,12	0,15	0,33	**0,31**	
	Cropland	4517,45	4347,73	4039,75	3836,16	3460,66	2859,71		**1657,74**
	Bare land	23,30	112,93	434,54	371,69	**786,42**	616,45		
6	**Built-up areas**	0,01	0,03	0,05	0,08	0,08	0,17	**0,16**	
	Cropland	4171,88	4084,37	3704,52	3427,42	3324,65	2999,21		**1172,66**
	Bare land	0,00	76,24	341,38	443,19	**614,87**	555,56		
7	**Built-up areas**	0,00	0,00	0,02	0,01	0,01	0,05	**0,05**	
	Cropland	3876,57	3846,09	3622,45	3477,33	3145,82	3200,35		**676,23**
	Bare land	26,42	85,55	261,35	362,38	**692,43**	400,67		

CONCLUSION

This study integrates Remote Sensing and GIS techniques with the Land Transfer Matrix (LTM), Multi-Buffer Ring (MBR), Standard Deviational Ellipse (SDE), Landscape Metrics (LM), and Contribution–Dependence Indices (CDI) to examine the spatial interactions among urban areas, cropland, and bare land, offering comprehensive insights into the cropland urbanization process. The findings reveal substantial urban expansion at an average annual rate of 28.3 ha/year, primarily at the expense of cropland, while also contributing to an increase in bare land. Urbanization followed a progressive Annual Urban Expansion Rate

(AUER), with cropland loss exhibiting a peak Annual Cropland Loss Rate (ACLR) during the early stages, indicating a strong correlation with the trajectory of urban growth. The observed rise in bare land, accompanied by fluctuating Annual Bare Land Increase Rate (ABLIR), suggests the influence of external factors such as agricultural abandonment or fallowing.

SDE results confirm directional spatial shifts across all land cover classes (with SDI values ≥ 0.5), signifying spatial reorganization. These dynamics reflect the continuous transformation of cropland and bare land into urban areas. The CDI analysis reveals a balanced but significant dependence of urbanization on both cropland and bare land: 89.4 % of urbanized bare land originated from former farmland, while approximately 25 % of cropland transitioned directly into urban land and 75% was first converted to bare land; of which 37.9 % was subsequently urbanized. SDE overlap analysis (SDE.OL) further supports these trends, showing stronger interactions between cropland and bare land than between urban areas and either of the other two land types. Increasing landscape fragmentation among the three land categories, as revealed by landscape metrics, corroborates the land conversion trends, while MBR analysis highlights rising urban density, declining cropland density, and increasing bare land presence in expanding urban zones. These patterns underscore the severity of unplanned urban growth and its implications for agricultural sustainability.

These findings confirm the influence of urban growth on cropland and bare land dynamics. With cropland loss accounting for 19 % of Tiaret’s fertile soils and increased fragmentation raising critical concerns about long-term food security. The results align with prior research identifying urban expansion as a principal driver of cropland decline. Although our rate results, as compared in the manuscript with those from other studies, are similar in magnitude, the extent and characteristics of urbanization vary across cities. This study underscores the interactions among built-up areas, cropland, and bare land, reveals the complex land cover dynamics of cropland urbanization, and highlights the underexamined role of bare land in this process. It offers an empirically grounded framework for assessing these dynamics, complementing previous research on cropland fragmentation under urbanization pressure, while also addressing related issues such as cropland damage from urban encroachment, declassification, and speculative land holding. This method provides empirical insight into the diffusion–coalescence process occurring during urbanization. Considering global land cover changes enables a comprehensive diagnosis of urban growth dynamics and an assessment of the associated environmental impacts. Such analysis contributes to understanding the current stage of urban development and provides valuable information for planners and policymakers to formulate appropriate and sustainable interventions. The findings further emphasise the need to manage bare land expansion in peripheral areas as a key planning challenge. Although focused on a medium-sized city, often underrepresented in urban studies, the implications warrant broader investigation across diverse urban contexts.

CONFLICT OF INTEREST

The authors declare that they have no competing interests.

REFERENCES

Abu Hatab, A., Cavinato, M.E.R., Lindemer, A., & Lagerkvist, C.-J. (2019). Urban sprawl, food security and agricultural systems in developing countries: A systematic review of the literature. *Cities*, *94*, 129–142. https://doi.org/10.1016/j.cities.2019.06.001

Abudu, D., Echima, R.A., & Andogah, G. (2019). Spatial assessment of urban sprawl in Arua Municipality, Uganda. *The Egyptian Journal of Remote Sensing and Space Science*, *22*(3), 315–322. https://doi.org/10.1016/j.ejrs.2018.01.008

Akın, A., & Erdoğan, M.A. (2020). Analysing temporal and spatial urban sprawl change of Bursa city using landscape metrics and remote sensing. *Modeling Earth Systems and Environment*, *6*(3), 1331–1343. https://doi.org/10.1007/s40808-020-00766-1

Banai, R., & DePriest, T. (2014). Urban Sprawl: Definitions, Data, Methods of Measurement, and Environmental Consequences. *Journal of Sustainability Education*, *7*.

Boori, M.S., Netzband, M., Choudhary, K., & Voženílek, V. (2015). Monitoring and modeling of urban sprawl through remote sensing and GIS in Kuala Lumpur, Malaysia. *Ecological Processes*, *4*(1), 15. https://doi.org/10.1186/s13717-015-0040-2

Bren d'Amour, C., Reitsma, F., Baiocchi, G., Barthel, S., Güneralp, B., Erb, K.-H., Haberl, H., Creutzig, F., & Seto, K.C. (2017). Future urban land expansion and implications for global croplands. *Proceedings of the National Academy of Sciences*, *114*(34), 8939–8944. https://doi.org/10.1073/pnas.1606036114

Chettry, V. (2023). A Critical Review of Urban Sprawl Studies. *Journal of Geovisualization and Spatial Analysis*, *7*(2), 28. https://doi.org/10.1007/s41651-023-00158-w

Dadashpoor, H., Azizi, P., & Moghadasi, M. (2019). Land use change, urbanization, and change in landscape pattern in a metropolitan area. *Science of The Total Environment*, *655*, 707–719. https://doi.org/10.1016/j.scitotenv.2018.11.267

Deng, J.S., Qiu, L.F., Wang, K., Yang, H., & Shi, Y.Y. (2011). An integrated analysis of urbanization-triggered cropland loss trajectory and implications for sustainable land management. *Cities*, *28*(2), 127–137. https://doi.org/10.1016/j.cities.2010.09.005

Dutta, I., & Das, A. (2019). Exploring the dynamics of urban sprawl using geo-spatial indices: A study of English Bazar Urban Agglomeration, West Bengal. *Applied Geomatics*, *11*(3), 259–276. https://doi.org/10.1007/s12518-019-00257-8

Eko, J., & Ayama, O.R. (2013). *Urban Sprawl Effects on Biodiversity in Peripheral Agricultural Lands in Calabar, Nigeria*. *3*.

Ewing, R. (1997). Is Los Angeles-Style Sprawl Desirable? *Journal of the American Planning Association*, *63*(1), 107–126. https://doi.org/10.1080/01944369708975728

Gomes, E., Banos, A., Abrantes, P., Rocha, J., Kristensen, S.B.P., & Busck, A. (2019). Agricultural land fragmentation analysis in a peri-urban context: From the past into the future. *Ecological Indicators*, *97*, 380–388. https://doi.org/10.1016/j.ecolind.2018.10.025

Gumma, M., Mohammad, I., Nedumaran, S., Whitbread, A., & Lagerkvist, C. (2017). Urban Sprawl and Adverse Impacts on Agricultural Land: A Case Study on Hyderabad, India. *Remote Sensing*, *9*(11), 1136. https://doi.org/10.3390/rs9111136

Hossain, A., Krupnik, T.J., Timsina, J., Mahboob, M.G., Chaki, A.K., Farooq, M., Bhatt, R., Fahad, S., & Hasanuzzaman, M. (2020). Agricultural Land Degradation: Processes and Problems Undermining Future Food Security. In S. Fahad, M. Hasanuzzaman, M. Alam, H. Ullah, M. Saeed, I. Ali Khan, & M. Adnan (Eds.), *Environment, Climate, Plant and*

Vegetation Growth (pp. 17–61). Springer International Publishing. https://doi.org/10.1007/978-3-030-49732-3_2

Li, H., Wang, C., Zhong, C., Su, A., Xiong, C., Wang, J., & Liu, J. (2017a). Mapping Urban Bare Land Automatically from Landsat Imagery with a Simple Index. *Remote Sensing*, *9*(3), 249. https://doi.org/10.3390/rs9030249

Li, S., Wang, T., & Yan, C. (2017b). Assessing the role of policies on land-use/cover change from 1965 to 2015 in the mu us sandy land, northern China. *Sustainability (Switzerland)*, *9*(7), 1–18. https://doi.org/10.3390/su9071164

Magidi, J., & Ahmed, F. (2019). Assessing urban sprawl using remote sensing and landscape metrics: A case study of City of Tshwane, South Africa (1984–2015). *The Egyptian Journal of Remote Sensing and Space Science*, *22*(3), 335–346. https://doi.org/10.1016/j.ejrs.2018.07.003

Mosammam, H.M., Nia, J.T., Khani, H., Teymouri, A., & Kazemi, M. (2017). Monitoring land use change and measuring urban sprawl based on its spatial forms. *The Egyptian Journal of Remote Sensing and Space Science*, *20*(1), 103–116. https://doi.org/10.1016/j.ejrs.2016.08.002

Paül, V., & Tonts, M. (2005). Containing Urban Sprawl: Trends in Land Use and Spatial Planning in the Metropolitan Region of Barcelona. *Journal of Environmental Planning and Management*, *48*(1), 7–35. https://doi.org/10.1080/0964056042000308139

Peerzado, M.B., Magsi, H., & Sheikh, M.J. (2019). Land use conflicts and urban sprawl: Conversion of agriculture lands into urbanization in Hyderabad, Pakistan. *Journal of the Saudi Society of Agricultural Sciences*, *18*(4), 423–428. https://doi.org/10.1016/j.jssas.2018.02.002

Qiu, B., Li, H., Tang, Z., Chen, C., & Berry, J. (2020). How cropland losses shaped by unbalanced urbanization process? *Land Use Policy*, *96*, 104715. https://doi.org/10.1016/j.landusepol.2020.104715

Raphael, O., & Ukandu, I. (2015). *Effect of Urbanization on Agricultural Production in Abia State*. *5*(2).

Ruiz-Lendínez, J.J. (2020). Abandoned Farmland Location in Areas Affected by Rapid Urbanization Using Textural Characterization of High Resolution Aerial Imagery. *ISPRS International Journal of Geo-Information*, *9*(4), 191. https://doi.org/10.3390/ijgi9040191

Sharma, M., Kumar, V., & Kumar, S. (2024). A systematic review of urban sprawl and land use/land cover change studies in India. *Sustainable Environment*, *10*(1), 2331269. https://doi.org/10.1080/27658511.2024.2331269

Song, X.-P., Hansen, M.C., Stehman, S.V., Potapov, P.V., Tyukavina, A., Vermote, E.F., & Townshend, J.R. (2018). Global land change from 1982 to 2016. *Nature*, *560*(7720), 639–643. https://doi.org/10.1038/s41586-018-0411-9

Tang, Z., Zhang, Z., Zuo, L., Wang, X., Zhao, X., Liu, F., Hu, S., Yi, L., & Xu, J. (2021). Spatial Evolution of Urban Expansion in the Beijing–Tianjin–Hebei Coordinated Development Region. *Sustainability*, *13*(3), 1579. https://doi.org/10.3390/su13031579

Tian, G., & Wu, J. (2015). Comparing urbanization patterns in Guangzhou of China and Phoenix of the USA: The influences of roads and rivers. *Ecological Indicators*, *52*, 23–30. https://doi.org/10.1016/j.ecolind.2014.11.024

Tiaret Wilaya. (2022, December 31). *Monograph of the Wilaya of Tiaret*.

Tu, Y., Chen, B., Yu, L., Song, Y., Wu, S., Li, M., Wei, H., Chen, T., Lang, W., Gong, P., & Xu, B. (2023). Raveling the nexus between urban expansion and cropland loss in China. *Landscape Ecology*, *38*(7), 1869–1884. https://doi.org/10.1007/s10980-023-01653-7

Tu, Y., Chen, B., Yu, L., Xin, Q., Gong, P., & Xu, B. (2021). How does urban expansion interact with cropland loss? A comparison of 14 Chinese cities from 1980 to 2015. *Landscape Ecology*, *36*(1), 243–263. https://doi.org/10.1007/s10980-020-01137-y

Turner, B.L., Lambin, E.F., & Reenberg, A. (2007). The emergence of land change science for global environmental change and sustainability. *Proceedings of the National Academy of Sciences*, *104*(52), 20666–20671. https://doi.org/10.1073/pnas.0704119104

United Nation. (2019). *World urbanization prospects: The 2018 revision*. United Nations.

Wang, Y., Zhao, F., Cheng, L., & Yang, K. (2015). Framework for monitoring the conversion of cultivated land to construction land using SAR image time series. *Remote Sensing Letters*, *6*(10), 794–803. https://doi.org/10.1080/2150704X.2015.1081304

Xie, Y., Hunter, M., Sorensen, A., Nogeire-McRae, T., Murphy, R., Suraci, J.P., Lischka, S., & Lark, T.J. (2023). U.S. Farmland under Threat of Urbanization: Future Development Scenarios to 2040. *Land*, *12*(3), 574. https://doi.org/10.3390/land12030574

Yameogo, C.E.W. (2021). Globalization, urbanization, and deforestation linkage in Burkina Faso. *Environmental Science and Pollution Research*, *28*(17), 22011–22021. https://doi.org/10.1007/s11356-020-12071-6

Yuan, Y., Chen, D., Wu, S., Mo, L., Tong, G., & Yan, D. (2019). Urban sprawl decreases the value of ecosystem services and intensifies the supply scarcity of ecosystem services in China. *Science of The Total Environment*, *697*, 134170. https://doi.org/10.1016/j.scitotenv.2019.134170

Yuan, Z., Zhou, L., Sun, D., & Hu, F. (2022). Impacts of Urban Expansion on the Loss and Fragmentation of Cropland in the Major Grain Production Areas of China. *Land*, *11*(1), 130. https://doi.org/10.3390/land11010130

Zhou, Y., Yang, G., Wang, S., Wang, L., Wang, F., & Liu, X. (2014). A new index for mapping built-up and bare land areas from Landsat-8 OLI data. *Remote Sensing Letters*, *5*(10), 862–871. https://doi.org/10.1080/2150704X.2014.973996